Dalton Transactions

ROYAL SOCIETY OF CHEMISTRY

PAPER

View Article Online
View Journal | View Issue

Cite this: *Dalton Trans.*, 2026, **55**, 205

Design of iron(III) phthalocyanine/reduced graphene oxide nanocomposites on nickel foam as hybrid supercapacitors

Nazlı Farajzadeh Öztürk, [a,b] Hacer Yasemin Yenilmez, †[a] Özlem Budak Doğramacı,†[c] Atıf Koca [c] and Zehra Altuntaş Bayır *[a]

It is well known that the position and number of substituents affect the electrochemical properties of electrodes *via* both altering the electropolymerization process and the redox activities of electropolymerized films. This study presents the synthesis of three new iron(III) phthalocyanines (**1–3**) bearing four or eight 9*H*-carbazol-2-yloxy groups at the non-peripheral or peripheral positions of the phthalocyanine ring. The newly synthesized macromolecules were characterized by performing spectroscopic techniques (FT-IR, UV-Vis, and MALDI-TOF) and used for the functionalization of graphene oxide nanosheets. Then, the surface of nickel foam (NiF) electrodes was modified with the resultant nanocomposites *via* a facile one-step electrodeposition strategy. During this process, the surface of the nickel foam electrodes was fabricated with a layer formed of simultaneous polymerization of iron(III) phthalocyanines and electrochemical reduction of graphene oxide. The supercapacitive properties of the prepared electrodes were examined and then compared with those of unmodified nickel foam, lone iron(III) phthalocyanine, and phthalocyanine/graphene oxide electrodes to study the synergistic effect of the electrode-forming species. All the hybrid electrodes showed higher supercapacitive performances. Among all the hybrid electrodes, the NiF/rGO$_2$-**1** electrode exhibited a higher specific capacitance of 590.4 F g^{-1} at 0.5 A g^{-1} compared to NiF/**1** (270.2 F g^{-1}). Furthermore, NiF/rGO$_2$-**1** displayed superior cycling stability, retaining 85.2% of its specific capacitance after 5000 continuous charge–discharge cycles, whereas NiF/**1** retained only 71.4%, highlighting the valuable effect of rGO decoration. Consequently, these metallophthalocyanine–reduced graphene oxide composites serve as promising agents for designing next-generation energy storage devices.

Received 28th August 2025,
Accepted 9th November 2025

DOI: 10.1039/d5dt02064f

rsc.li/dalton

Introduction

Generally, batteries have a limited cycle life, higher charging time, lower power density, are environmentally unsafe, and have heating problems. Some new alternatives have been designed to overcome these drawbacks. Supercapacitors are among the largest capacitive agents exhibiting the applicable features of batteries and capacitors in an energy storage system.[1] The occurrence of charge separation between the electrode and the electrolyte results in storage and energy delivery at a relatively higher rate than that of batteries. A supercapacitor is formed of an electrolyte, two electrodes, and a separator to isolate the electrodes electrically. Two principal mechanisms control the charge-storage efficiency of a supercapacitor: (1) electric double-layer capacitance (EDLC) based on electrostatic interactions and (2) pseudocapacitance based on chemical reactions.[2,3]

The materials used for the formation of supercapacitor electrodes play a vital role in the design of an efficient supercapacitor with a long life, flexible packaging, low weight, low maintenance, and high power. Moreover, the electrochemical properties of the electrode materials significantly depend on the electrical conductivity, wetting of electrodes, surface area, and permeability of the electrolyte. To improve the low energy density of a supercapacitor, some new electrode materials have been developed using carbon-, metal complex-, and polymer-based systems. Carbon materials provide a high surface area, whereas metal complexes display low resistance and specific capacitance to obtain powerful supercapacitive devices. In these structures, polymers can manage redox processes for

[a]*Department of Chemistry, Istanbul Technical University, TR-34469 Istanbul, Türkiye. E-mail: bayir@itu.edu.tr*
[b]*Department of Analytical Chemistry, Faculty of Pharmacy, Acıbadem Mehmet Ali Aydınlar University, Ataşehir, TR-34752 Istanbul, Türkiye*
[c]*Department of Chemical Engineering, Engineering Faculty, Marmara University, Istanbul, Türkiye*
† These authors contributed equally to this work.

storage/release charge as well.[4] Recently, the potential and possibility of paramagnetic metal-containing phthalocyanines to prepare suitable supercapacitive electrodes have been studied owing to their excellent conductivity and electrochemical performance.[5–10]

A phthalocyanine ring is formed of four indole units with a vacant center being inserted into diverse metal cations to synthesize metal phthalocyanines.[11–13] Also, the periphery of the phthalocyanine ring can be altered by the addition of long and bulky groups *via* aromatic substitution reactions. Although metal ions and substituents refine the solubility of phthalocyanines by diminishing aggregation, they can modify unique features (*e.g.*, electrical, chemical, and physical) of these structures.[14–16] For instance, iron-based materials exhibit excellent electrochemical performance that can be combined with their chemical and mechanical properties to design and develop efficient electrochemical devices. Besides, polymerizable groups can be selected to alter the ring periphery.[17–19] Among these groups, carbazoles demonstrate charge carrier mobility, high quantum yields, and photochemical stability. In particular, homopolymerization of carbazoles shows high electrochemical stability and conductivity depending on the switching time, band gap, coloration efficiency, and optical contrast.[20] Carbazole polymers form stable radical cations and have hole-transferring capability and thermal stability.[21,22] Additionally, electropolymerization of carbazoles from 3 and 6 positions has been reported in the literature.[23]

Nontoxicity, low price, versatile availability, environmental friendliness, and high stability make carbon-based structures suitable materials to fabricate supercapacitor electrodes. Charge storage in pure carbon systems is achieved through electrostatic interactions; however, it is associated with chemical reactions in modified carbon structures. In particular, reduced graphene oxide nanosheets have been of interest in recent years to design novel pseudocapacitors with higher chemically reactive charge-storage performance.[2] Among them, transition metal-containing structures have been considered potent alternatives for pseudocapacitors. The resultant composites can store charges *via* electrostatic interactions and chemical reactions.[24]

In this study, three peripherally or non-peripherally substituted iron(III) phthalocyanines bearing electropolymerizable groups were synthesized and used to prepare phthalocyanine/reduced graphene oxide nanocomposites through a one-step electrochemical process. The resultant nanostructures were fabricated on nickel foam electrodes using a one-step cyclic voltammetry method. The simultaneous electropolymerization of the carbazole-containing phthalocyanines and electrodeposition of reduced graphene oxides on the nickel foam substrate overcame the disadvantages of binders on the electrodes. The rich redox activities of the iron(III) phthalocyanines were promoted by electropolymerizable carbazole substituents exhibiting high redox activity to achieve high pseudocapacitance. Besides, the preparation of the binder-free electrodes resolved the loss of pseudocapacitance performance originating from the low conductivity of the polymeric binder. Also, reduced graphene oxide- and iron(III) phthalocyanine-containing electrodes were prepared, and their electrochemical features were investigated to study the synergistic effect of iron(III) phthalocyanines and reduced graphene oxide nanosheets on the supercapacitance of the hybrid electrodes. The influence of the position and number of carbazole substituents was also investigated in this study. To examine the supercapacitive properties of the prepared hybrid electrodes, cyclic voltammetry (CV), galvanostatic charge–discharge (GCD), and electrochemical impedance spectroscopy (EIS) were applied. Consequently, this work investigates the potential of iron(III) phthalocyanine–reduced graphene oxide electrodes for supercapacitor applications. Compared to high-performance electrodes, the combination of these materials may offer advantages, as it could improve charge transfer and ion diffusion, leading to enhanced electrochemical properties. Furthermore, incorporating iron(III) phthalocyanine–reduced graphene oxide with other high-performance materials may refine device performance by overcoming their limitations and further the application of this strategy for advanced supercapacitors.

Experimental

Phthalonitrile derivatives (**a–c**) were prepared according to the method that has been extensively explained in the literature[25] with some modifications. Briefly, 3-nitro phthalonitrile, 4-nitro phthalonitrile, or 4,5-dichlorophthalonitrile and 9*H*-carbazol-2-ol were dissolved in DMF or DMSO and stirred for 24–48 hours. The related reaction was catalyzed in the presence of potassium carbonate. The content was poured into an ice : water mixture and recrystallized from ethanol.

Synthesis and characterization

General synthetic procedure for iron(III) phthalocyanines (1–3). 100 mg of each phthalonitrile derivative (**a** and **b**: 0.324 mmol; **c**: 0.200 mmol) and iron(II) acetate (for **a** and **b**: 19 mg, 0.10 mmol; for **c**: 9.0 mg, 0.050 mmol) were dissolved in *N*,*N*-dimethylamino methanol (2 mL) at reflux temperature for 24 hours under an inert atmosphere. The reaction content was cooled to room temperature, poured into an ice/water mixture (80 mL), and stirred for one hour. The precipitate was filtered off and washed several times with hot *n*-hexane. The pure product was obtained by performing a chromatographic technique on silica gel as the stationary phase and tetrahydrofuran (for **a** and **b**) or *n*-hexane : tetrahydrofuran (2 : 1) (for **c**) as the eluent.

*FePc (**1**).* Yield: 0.048 g (44%), m. p. > 250 °C. FT-IR cm^{-1}: 3328 (N–H), 3071 (Ar–H), 1603 (C=O), 1459, 1240, 1119, 1052. MALDI TOF-MS: *m*/*z* calculated $[M]^+$ 1352.20; found 1290.62 $[M-Ac-3]^+$. UV-vis (THF): λ_{max} nm (log ε) 327 (5.30), 710 (5.10).

*FePc (**2**).* Yield: 0.041 g (38%), m. p. > 250 °C. FT-IR cm^{-1}: 3327 (N–H), 3043 (Ar–H), 1591 (C=O), 1457, 1233, 1116, 1090. MALDI TOF-MS: *m*/*z* calculated $[M]^+$ 1352.20; found 1293.62 $[M-Ac]^+$. UV-vis (THF): λ_{max} nm^{-1} (log ε) 327 (5.22), 697 (5.06).

*FePc (**3**).* Yield: 0.044 g (42%), m. p. > 250 °C. FT-IR: cm^{-1} 3389 (N–H), 3046 (Ar–H), 1678 (C=O), 1110 (C–O–C). MS (MALDI-TOF): *m*/*z* calculated $[M]^+$ 2076.95; found 2014.88

$[M-Ac-3H]^+$. UV-vis (DMSO): λ_{max} nm^{-1} ($\log \varepsilon$) 331 (5.47), 670 (5.08).

Electrochemical and supercapacitive studies

Materials. Graphite powder (Acros-organics), sulphuric acid (Aldrich), phosphoric acid (Merck), potassium permanganate (Sigma–Aldrich), and hydrogen peroxide (30%, Aldrich) were used to prepare graphene oxide. Each compound (**1–3**) and graphene oxide were dispersed in the electrodeposition solution (acetonitrile (AN) (Carlo Erba)/tetrabutyl ammonium perchlorate (TBAP) (Fluka Analytical)) to produce the hybrid structures. Ni foam (NiF, 1.6 mm in thickness) used as a substrate was provided by the MTI KJ Group. Potassium hydroxide (Merck) was used to prepare the electrolyte solution for the examination of electrochemical performance. Acetone (Isolab), absolute ethanol (Merck), and deionized water (DI) were utilized to clean the Ni foam before electrodeposition.

Preparation of tested electrodes. Before electrodeposition, Ni foam sheets (substrates: 1 cm^2 × 1 cm^2) were rinsed by sonication with acetone, deionized water (DI), and ethanol for 15 minutes and dried at room temperature. The electrodeposition solution was prepared in acetonitrile (AN) using 0.1 mol dm^{-3} of each iron(III) phthalocyanine (FePc; **1–3**) with an equivalent concentration of tetrabutyl ammonium perchlorate (TBAP). NiF/FePc electrodes were prepared by performing the repetitive cyclic voltammetry (rCV) technique. In a three-electrode system, Ni foam was used as the working electrode, Pt wire as the counter electrode, and Ag/AgCl as the reference electrode. The rCV process was performed at a scan rate of 100 mV s^{-1} for 10 cycles within the voltage range of 0–1.2 V *vs.* Ag/AgCl. The as-fabricated electrodes underwent an annealing procedure in a horizontal tube furnace under an Ar atmosphere at 100 °C for 1 hour. The same procedure was used for the preparation of NiF/rGO_2-FePc hybrid electrodes, except that the electrodeposition solution included a GO/FePc mixture. The GO/FePc ratio of 40/60 was chosen based on our previous study, which suggests that this composition provided the highest specific capacitance and stability.[7] After ensuring the good dispersion of the solution, the rCV process was performed at a scan rate of 100 mV s^{-1} for 10 scans within the potential range of −1.8–1.4 V *vs.* Ag/AgCl. The annealing step was conducted under the same conditions as for the NiF/FePc electrodes.

Electrochemical measurements. The electrochemical analyses of the fabricated electrodes were conducted using a three-electrode cell set-up (Reference 1000B Potentiostat/Galvanostat/ZRA). The hybrid structures synthesized directly on Ni foam were used as the working electrodes. For all the studies, the Pt wire and saturated calomel electrode (SCE) served as the counter and reference electrodes, respectively. All the electrodes were immersed in 2 mol dm^{-3} potassium hydroxide solution during the electrochemical performance tests. Cyclic voltammetry (CV) analyses were performed at different scan rates ranging from 10 to 50 mV s^{-1} to examine the redox properties of the electrodes. Galvanostatic charge/discharge (GCD) tests were performed at various discharge current densities ranging from 0.5 A g^{-1} to 10 A g^{-1} to determine the specific capacitance of the prepared electrodes. Cycling stability measurements were performed at a current density of 10 A g^{-1} for repetitive 5000 charge/discharge cycles. Electrochemical impedance spectroscopic (EIS) tests were conducted in a frequency range of 10^5–10^{-1} Hz at a constant amplitude of 10 mV.

The specific capacitance (C_s) of the fabricated electrodes was calculated using the following equation:[26]

$$C_s = (I \times \Delta t)/(\Delta V \times m) \quad (1)$$

where C_s is the specific capacitance (F g^{-1}), I is the discharge current (A), Δt is the discharge time (s), and m is the mass loading of the active material on NiF (g).

Results and discussion

Synthesis and characterization

The synthetic route for compounds **1–3** is presented in Scheme 1. Phthalonitrile derivatives (**a–c**) were prepared as described in the literature[25] and used to synthesize compounds **1–3**. Cyclotetramerization of each phthalonitrile in the presence of iron(II) acetate in *N*,*N*-dimethyl amino ethanol resulted in the synthesis of the related iron(III) phthalocyanine through a one-step template mechanism. The resultant phthalocyanines were characterized using FT-IR, UV-vis, and MALDI-TOF spectroscopic approaches. The obtained data confirmed the successful synthesis of the predicted structures.

Electrochemical and supercapacitive studies

To analyze the supercapacitive features of compounds **1–3**, their electron transfer capacities and electrochemical reaction mechanisms were evaluated by applying CV and square wave voltammetry (SWV) in a three-electrode configuration (glassy carbon electrode (GCE): the working electrode; Pt wire: the counter electrode; Ag/AgCl electrode: the reference electrode). While all the compounds exhibited similar electrochemical responses, slight variations were observed in their peak potentials and reversibility of electron transfer reactions. These different voltammetric responses indicated that the position and number of the substituents influenced the redox responses of the phthalocyanine ring (Pc ring) and the metal center owing to the different electron-releasing ability of the substituents. According to the voltammetric responses of complexes **1–3**, the presence of 9*H*-carbazol-2-yloxy substituents at the non-peripheral positions of the Pc ring led to an increase in the electron density of the Pc ring. Indeed, the proximity of the substituent to the Pc center in compound **1** increased its tendency to donate electrons and, in turn, affected the ease of the electron transfer reactions of the Pc ring.

To provide a detailed illustration, the electrochemical characterization of compound **1** was selected as a representative example. Accordingly, the CV and SW measurements performed in AN/TBAP for compound **1** are illustrated in Fig. 1. Notably, compound **1** displayed four characteristic reduction

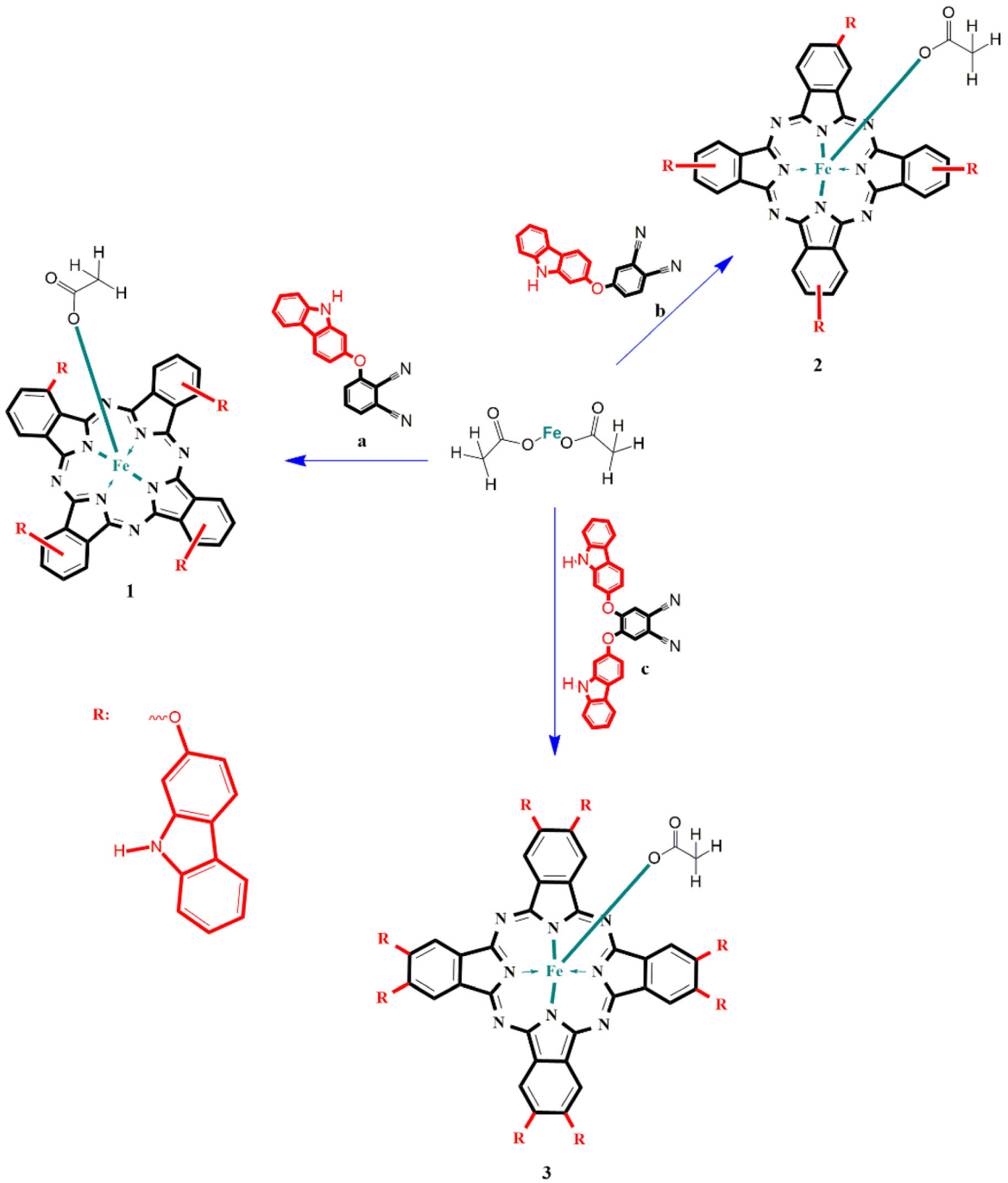

Scheme 1 Synthetic procedure for compounds **1–3**; *N*,*N*-dimethylamino methanol, reflux temperature, 24 hours.

peaks at −0.12 V (Red1), −0.48 V (Red2), −0.83 V (Red3), and −1.12 V (Red4), along with two oxidation peaks at 0.54 V (Oxd1) and 0.98 V (Oxd2) in the presence of AN/TBAP medium. The Red1 and Oxd1 were attributed to the reduction and oxidation of the metal center, respectively. On the other hand, the remaining processes were assigned to the Pc-based reduction processes occurring within the negative potential range. The ratio of the anodic peak current to the cathodic peak current ($I_{p,a}/I_{p,c}$) and the peak-to-peak separation responses (ΔE_p) of the redox couples revealed that the reduction processes were both electrochemically and chemically reversible. Besides, the Oxd2 resulted in a relatively higher peak current compared to Oxd1 and an irreversible response, which could be associated with the cationic electropolymerization of compound **1** on the Ni foam surface through the oxidation of the carbazole substituents.[27,28] Based on the recorded voltammetric responses, an increase in the scan rate did not significantly change the reversibility (Fig. 1a). Consequently, compound **1**,

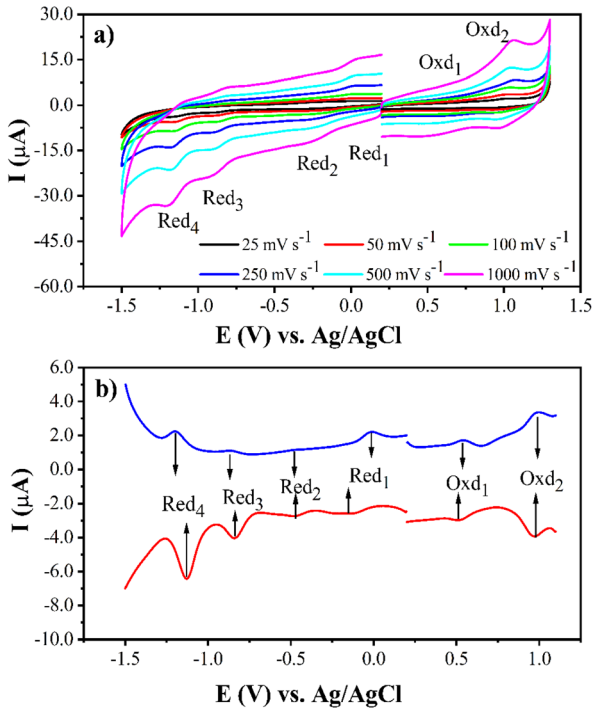

Fig. 1 Voltammograms of compound **1** recorded at different scan rates on a GCE working electrode in AN/TBAP: (a) CVs and (b) SWVs.

including four substituents at non-peripheral positions, displayed favorable electrochemical properties, making it a promising active material for supercapacitors. The CV experiments also supported the good reversibility of these reduction and oxidation processes by applying various vertex potentials (Figure S1). The voltammetric responses of compounds **2** and **3** are depicted in Figures S2–5.

The FePc and rGO_2-FePc composite structures were directly synthesized on the NiF surface *via* one-step repetitive cyclic voltammetry (rCV). The responses of the electrodeposition processes of nickel foam/iron(III) phthalocyanine (NiF/**1**) and nickel foam/iron(III) phthalocyanine–reduced graphene oxide NiF/rGO_2-**1** are demonstrated in Fig. 2. For the preparation of the NiF/**1** electrode, the rCV technique was applied within the potential range of 0–1.2 V *vs.* Ag/AgCl for 10 cycles. Due to the cationic electropolymerization of the carbazole groups, two oxidation peaks were detected at 0.60 V and 1.02 V, respectively (Fig. 2a). The increase in peak currents during the rCV scans can be assigned to the growth of compound **1** on the NiF surface. The insoluble film formed by electrodeposition on the NiF surface was visibly observed with the naked eye. The potential window was set between −1.8 V and 1.4 V for the simultaneous electropolymerization of compound **1** and electrochemical reduction of GO to rGO to obtain NiF/rGO_2-**1**. Although the first peak was observed at 1.01 V, it then shifted to 0.66 V. The electropolymerization of compound **1** on the NiF surface was confirmed by increasing the peak currents during consecutive rCV scans. Furthermore, a peak was recorded at approximately −0.95 V, which could be attributed to the electrochemical reduction of GO to rGO. On the other hand, the decrease in the current of this peak could originate from an irreversible reduction process during the rCV scans. These voltammetric results were in good agreement with the literature.[7,8,29] Besides, the peak current intensities of electro-

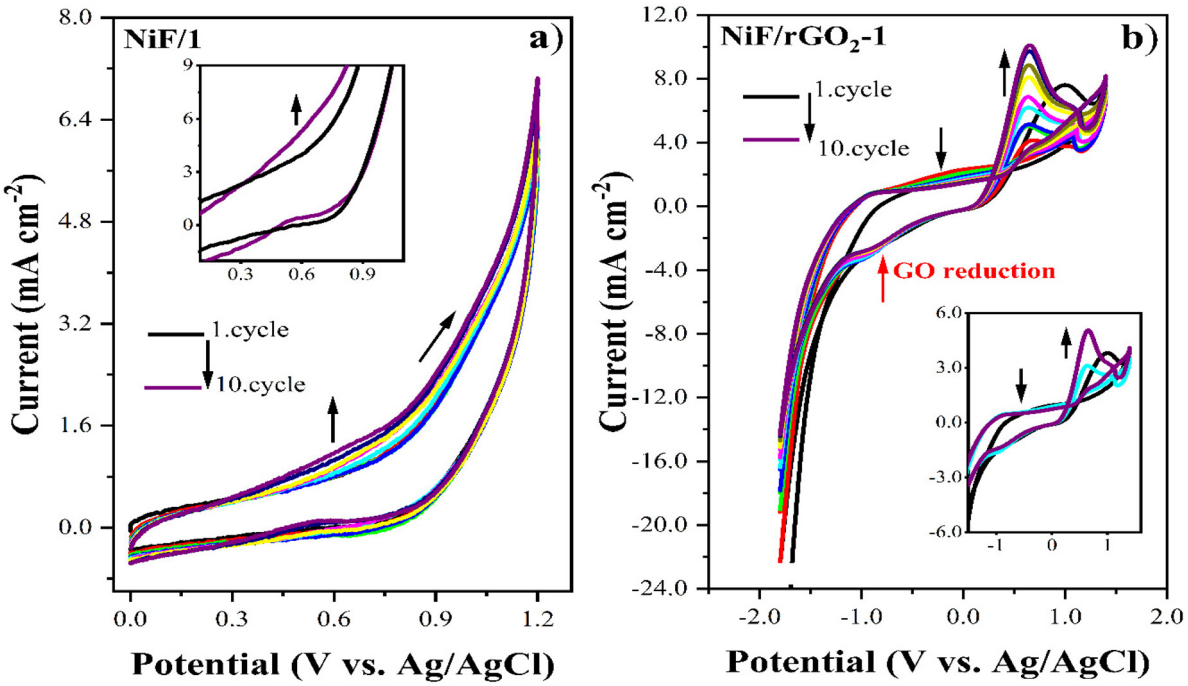

Fig. 2 rCV scans of (a) NiF/**1** and (b) NiF/rGO_2-**1** electrodes at a scan rate of 100 mV s^{-1} in the AN/TBAP medium.

deposition increased in the presence of GO (Fig. 2b). The electrodeposition profiles of NiF/**2**, NiF/rGO$_2$-**2**, NiF/**3**, and NiF/rGO$_2$-**3** electrodes are depicted in Figure S6 and S7.

The Fourier-transform infrared (FTIR) spectra of the NiF/**1** and NiF/rGO$_2$-**1** films are shown in Fig. 3a. The typical peaks observed at 731, 1085, 1380, and 1458 cm^{-1} corresponded to phthalocyanine skeletal vibrations.[8] Furthermore, the signal detected at 824 cm^{-1} originated from metal–ligand vibrations in FePc. The signal of the C=O group appeared at 1742 cm^{-1}. The stretching vibrations of CH_3 and CH_2 observed at 2973 and 2878 cm^{-1} were assigned to the existence of rGO. The broad band at 3340 cm^{-1} was further ascribed to –OH groups associated with rGO in the hybrid structure. In addition, the incorporation of rGO resulted in a noticeable increase in the intensities of these peaks. The crystal structure of the fabricated films on NiF was also characterized using X-ray diffraction spectroscopy (XRD). Fig. 3b presents the XRD patterns of the as-prepared NiF/**1** and NiF/rGO$_2$-**1** electrodes, in which three distinct peaks (45.4°, 52.7°, and 76.9°) matched Ni (JCPDS no. 04-0850).[30] The characteristic peaks of compound **1** and rGO$_2$-**1** were not distinguished due to the relatively high intensity peaks arising from NiF. However, the broad peak observed at 20.1° confirmed the presence of rGO in the hybrid structure.[31]

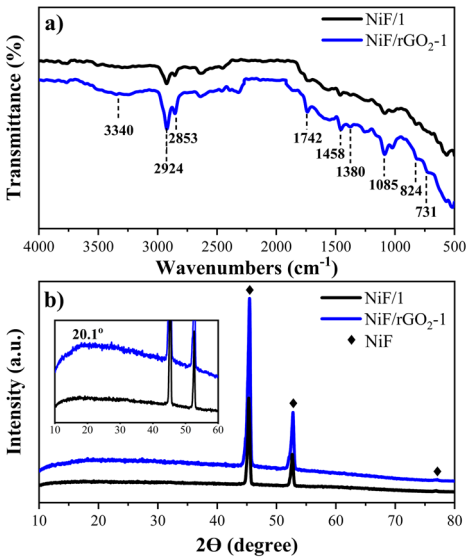

Fig. 3 Structural characterization of NiF/**1** and NiF/rGO$_2$-**1** electrodes: (a) FTIR spectra and (b) XRD patterns.

The morphologies of the NiF/**1** and NiF/rGO$_2$-**1** electrodes are illustrated in Fig. 4. Compound **1** resulted in a smooth surface with some agglomerated particles (Fig. 4a); however, the rGO$_2$-**1** composite had a relatively uniform and non-agglomerated surface compared to compound **1** (Fig. 4b). As shown in Fig. 4c, the electrodeposited film of compound **1** also contained spherical particles. Moreover, the 2D structure of rGO sheets was clearly visible on the NiF surface. These observations suggested that the presence of the 2D structure of rGO contributed to the formation of a smoother surface and a noticeable increase in porosity, which may enhance the energy storage capacity of the electrode. In the EDS spectra, the signals corresponding to Fe, C, O, and N verified the successful growth of the targeted film on the NiF surface. Additionally, the Ni peaks detected in the spectrum originate

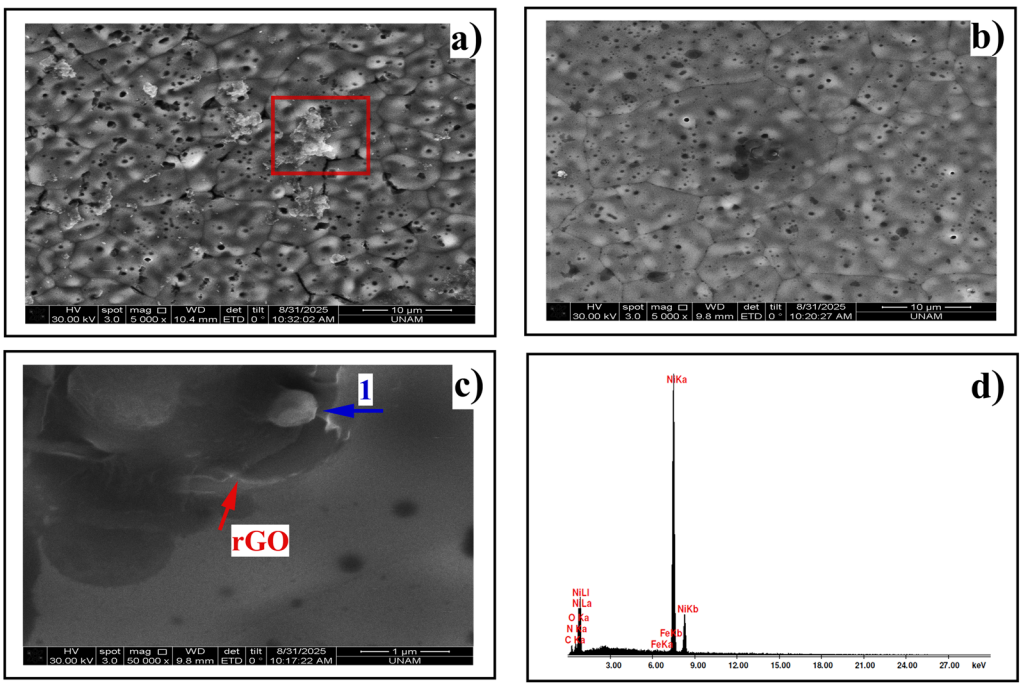

Fig. 4 SEM images at 5000× of (a) NiF/**1** and (b) NiF/rGO$_2$-**1**; (c) SEM image of NiF/rGO$_2$-**1** at 50 000×; (d) EDS results of NiF/rGO$_2$-**1**.

from the substrate (Fig. 4d). The results obtained were in accordance with the FTIR findings, indicating the successful growth of the sample on NiF.

To study the electrochemical performance of the fabricated electrodes, CV, GCD, and EIS measurements were conducted in a solution of potassium hydroxide (2.0 mol dm^{-3}) using a three-electrode configuration. Fig. 5a illustrates the CV curves of all the electrodes at a scan rate of 20 mV s^{-1} within the potential range of 0–0.5 V *vs.* SCE. Due to reversible faradaic reactions, the CV curves displayed well-defined redox pairs positioned between 0.20 and 0.45 V. Compared to the other electrodes, the NiF/rGO_2-**1** electrode possessed a larger integrated area under the curve, leading to higher specific capacitance. Additionally, hybrid structures fabricated with rGO exhibited larger integrated areas than bare composites. Indeed, the existence of rGO in the hybrid structure improved the performance of the electrodes by providing better conductivity and a higher surface area. Galvanostatic charge–discharge (GCD) analyses were performed to study the charge storage properties of these electrodes. Fig. 5b presents the GCD profiles of the electrodes at a constant discharge current density of 0.5 A g^{-1} within the potential window of 0–0.5 V. The extended discharge time of the NiF/rGO_2-**1** hybrid electrode verified the improved specific capacitance, supporting the results of the CV tests. The respective specific capacitance values of NiF/**1**, NiF/**2**, NiF/**3**, NiF/rGO_2-**1**, NiF/rGO_2-**2**, and NiF/rGO_2-**3** were 270.2, 228.8, 218.4, 590.4, 481.6, and 426.2 F g^{-1} at a current density of 0.5 A g^{-1} (Fig. 5c). rGO significantly improved the specific capacitance performance of the electrodes due to its remarkably higher conductivity and improved charge transfer ability. The remarkable performance differences of these electrodes could result from the electrochemical properties of the FePc complexes. In compound **1**, the presence of substituents at the non-peripheral positions of the Pc ring enhanced its electron density, which in turn shifted the oxidation potentials to less positive values and influenced its capacitance.

The Nyquist plots reveal the internal resistance (R_s) between the electrode material and the electrolyte, the charge transfer resistance (R_{ct}) associated with faradaic reactions, and the Warburg resistance (W) originating from diffusion resistance.[32,33] The resistance values of all the prepared electrodes are listed in Table S1. The obtained R_{ct} values were relatively small for all electrodes. As shown in Fig. 5d, the Nyquist

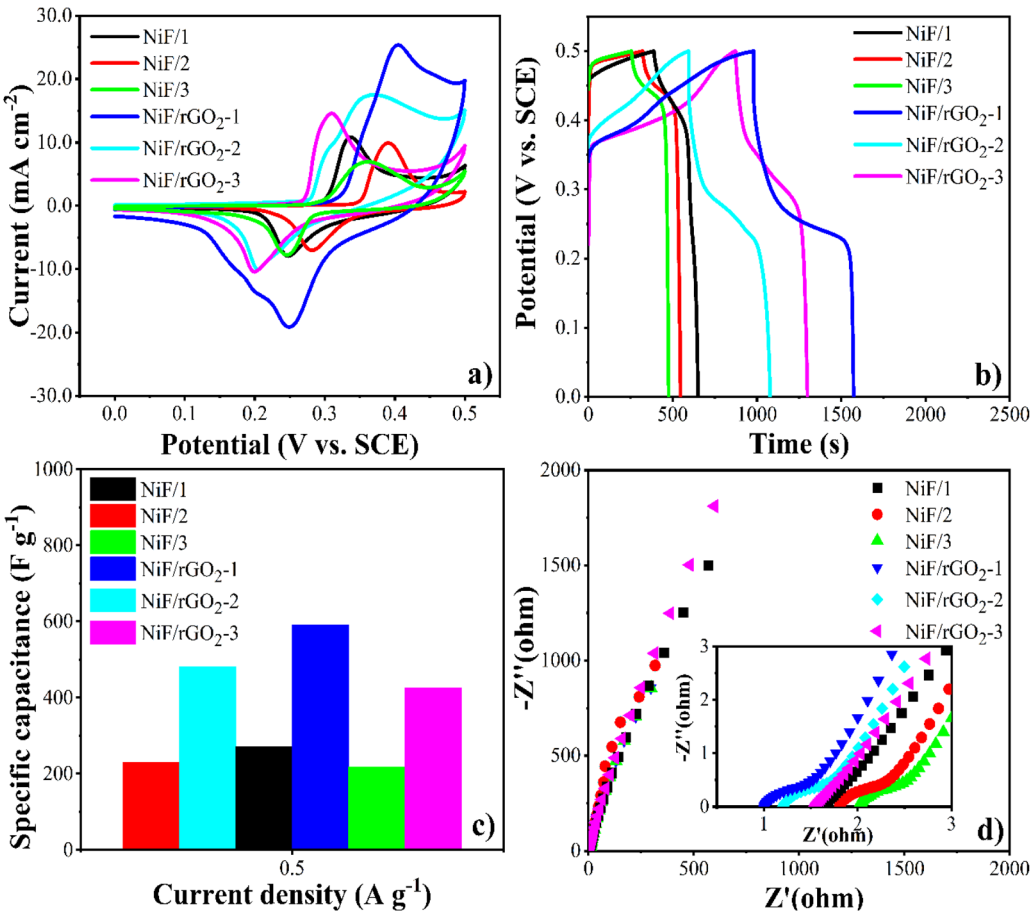

Fig. 5 Comparison of the fabricated electrodes: (a) CV profiles at 20 mV s^{-1}; (b) GCD curves at 0.5 A g^{-1}; (c) specific capacitance values at 0.5 A g^{-1}; and (d) Nyquist plots in the frequency range of 100 kHz–0.1 Hz.

plots displayed a semicircle in the high-frequency region and a straight line in the low-frequency region. On the other hand, NiF/rGO_2-**1** exhibited the lowest R_s of 1.0 Ω, and the slope of W was also the highest, indicating the highest electrochemical performance. As a result, the interaction between compound **1** and rGO led to the lowest resistance for NiF/rGO_2-**1**, which was also supported by the GCD measurements.

The electrochemical properties of the NiF/rGO_2-**1** composite electrode are thoroughly examined to assess its commercial potential for supercapacitor applications (Fig. 6). The CV profiles recorded at various scan rates ranging from 10 to 50 mV s^{-1} revealed that the charge transfer mechanism of NiF/rGO_2-**1** depended on faradaic redox reactions (Fig. 6a). The oxidation and reduction peaks shifted slightly by increasing scan rates and fast redox reactions. Thus, NiF/rGO_2-**1** maintained its stability even at 50 mV s^{-1} and exhibited a high rate capability. GCD tests were performed at different discharge current densities ranging from 0.5 to 10 A g^{-1} to determine the specific capacitance values of NiF/rGO_2-**1** (Fig. 6b). The almost symmetric GCD curves verified the high rate capability of the NiF/rGO_2-**1** hybrid electrode. Additionally, the triangular shape of the GCD curves was in good agreement with the pseudocapacitive behavior observed in the CV profiles. The specific capacitance values of NiF/rGO_2-**1** were 590.4, 494.8, 428.2, 396.4, 350.0, and 312.8 F g^{-1} at 0.5, 1, 2, 3, 5, and 10 A g^{-1}, respectively (Fig. 6c). The specific capacitance of NiF/rGO_2-**1** was higher than the values reported in the literature.[34–37] The decrease in specific capacitance values at higher current densities could be attributed to the diffusion resistance between the electrolyte ions and the active material on the NiF surface. The NiF/rGO_2-**1** hybrid electrode possessed approximately double-folded specific capacitance compared to NiF/**1** owing to the refining role of rGO in the hybrid electrodes. The cycling stability of NiF/rGO_2-**1** was evaluated using repetitive GCD measurements. Fig. 6d illustrates the cycling stability performance of NiF and NiF/rGO_2-**1** over 5000 cycles at 10 A g^{-1}. The respective remaining stability was 71.4% and 85.2% for NiF and NiF/rGO_2-**1**, supporting the enhanced electrochemical properties of NiF/rGO_2-**1** due to the presence of rGO. A comparison of the supercapacitive performance of the NiF/rGO_2-**1** hybrid electrode with the previously reported studies is presented in Table S2. As a result, the composites composed of the newly synthesized iron(III) phthalocyanines and rGO can be considered potential nanocomposites for supercapacitive applications.

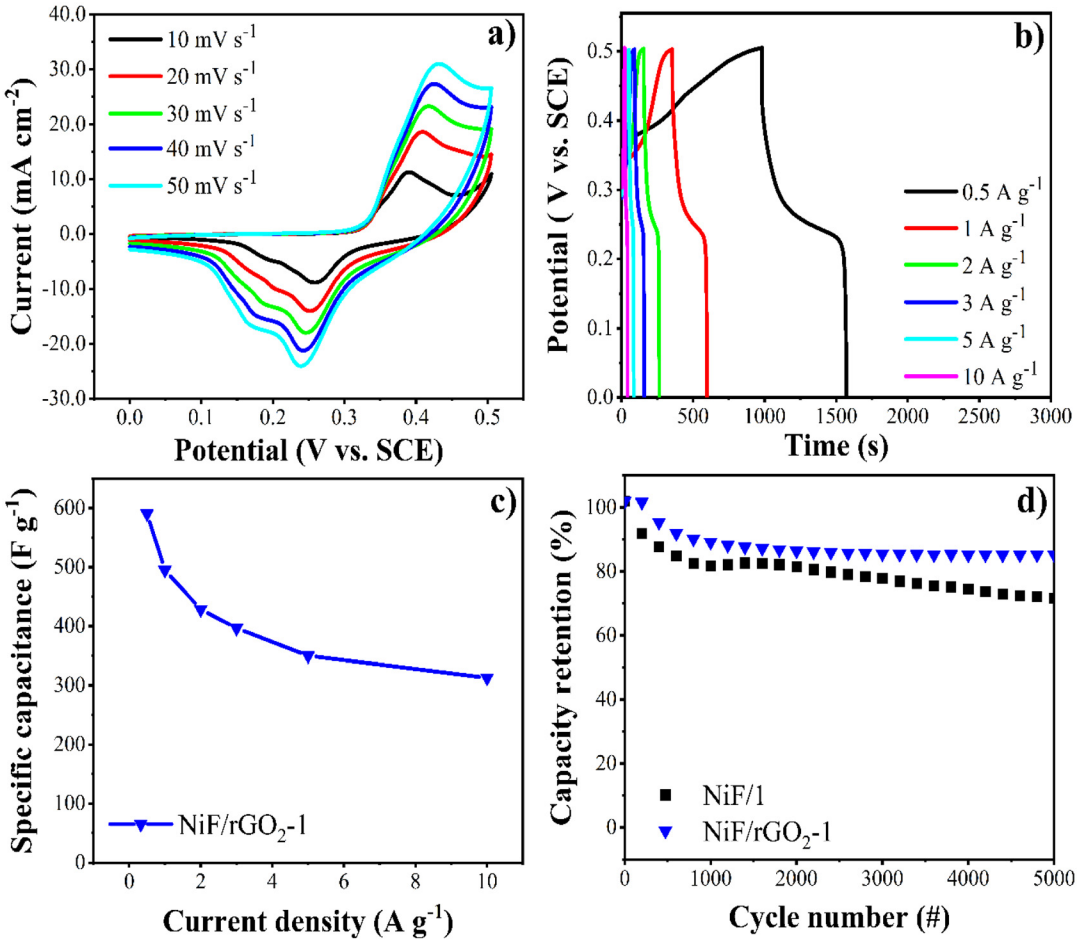

Fig. 6 Electrochemical properties of NiF/rGO_2-**1**: (a) CV curves at several scan rates (10–50 mV s^{-1}); (b) GCD curves at various discharge current densities (0.5–10 A g^{-1}); (c) specific capacitances depended on discharge current densities; and (d) cycling stability at 10 A g^{-1} for 5000 cycles.

Conclusions

In this study, new non-peripherally tetra-substituted, peripherally tetra-substituted, and peripherally octa-substituted iron(III) phthalocyanines were successfully synthesized and structurally characterized. By employing these novel structures, iron(III) phthalocyanine–reduced graphene oxide hybrids were successfully obtained on the NiF surface through a simple one-step electrodeposition process. The impressive electrochemical performance of the fabricated hybrid electrodes can be assigned to the synergistic incorporation of iron(III) phthalocyanine as a pseudocapacitive material and rGO as a highly conductive support. The non-peripherally iron(III) phthalocyanine–reduced graphene oxide hybrid, NiF/rGO_2-**1**, exhibited superior supercapacitive properties, delivering a high specific capacitance of 590.4 F g^{-1} at 0.5 A g^{-1} and improved cycling stability, retaining 85.2% of its initial specific capacitance at 10 A g^{-1} after 5000 repetitive cycles. This study revealed that the suggested hybrid structures, composed of iron(III) phthalocyanine–reduced graphene oxide, can be regarded as potential alternative electrode active materials for supercapacitor applications by enhancing electrochemical performance.

Conflicts of interest

There are no conflicts to declare.

Data availability

The data that support the findings of this study are available from the corresponding author upon reasonable request.

Supplementary information (SI) is available. See DOI: https://doi.org/10.1039/d5dt02064f.

Acknowledgements

This study was financially supported by the Scientific and Technological Research Council of Türkiye (TÜBİTAK) under Grant Number 122Z036.

References

1 J. P. Zheng, *J. Electrochem. Soc.*, 2005, **152**, A1864.
2 P. V. Adhyapak, T. Maddanimath, S. Pethkar, A. J. Chandwadkar, Y. S. Negi and K. Vijayamohanan, *J. Power Sources*, 2002, **109**, 105.
3 M. Yoshio, H. Nakamura and H. Wang, *Electrochem. Solid-State Lett.*, 2006, **9**, A561.
4 P. Sharma and T. S. Bhatti, *Energy Convers. Manage.*, 2010, **51**, 2901.
5 N. Y. P. Kumar, Mounesh, T. M. Sharanakumar and K. R. Venugopala Reddy, *Chem. Pap.*, 2021, **75**, 2683.
6 M. B. Arvas, S. Yazar and Y. Sahin, *J. Alloys Compd.*, 2022, **919**, 165689.
7 H. Y. Yenilmez, O. Budak, N. F. Öztürk, A. Koca, A. Boz, B. Ustamehmetoglu and Z. A. Bayir, *Dalton Trans.*, 2024, **53**, 1766.
8 Ö. Budak, N. F. Öztürk and A. Koca, *Mater. Sci. Semicond. Process.*, 2025, **188**, 109254.
9 J. Mu, Y. Zhao, Z. Guo, Z. Zhang, H. Che, Y. Wang, X. Zhang, G. Wang, J. Mu and L. Wang, *J. Energy Storage*, 2023, **61**, 106768.
10 W. Chen, M. Fu, S. Yang, L. Ning, H. Yu, M. Gao, K. Wang, M. Guan, R. Lv, N. Li and J. Pan, *Chem. Eng. J.*, 2025, **514**, 163341.
11 C. C. Leznoff and A. B. P. Lever, *Phthalocyanines Properties and Applications*, VCH, New York, 1989, 1993 and 1996, vol 1–4.
12 Ö. Bekaroğlu, *Appl. Organomet. Chem.*, 1996, **10**(8), 605.
13 Z. A. Bayır, *Dyes Pigm.*, 2005, **65**(3), 235.
14 C. Uslan, K. T. Oppelt, L. M. Reith, B. Ş. Sesalan and G. Knör, *Chem. Commun.*, 2013, **49**, 8108.
15 Ş. Özçelik, A. Koca and A. Gül, *Polyhedron*, 2012, **42**(1), 227.
16 E. T. Saka, R. Z. U. Kobak, H. Alp, G. Sarkı, A. Koca and H. Kantekin, *Synth. Met.*, 2016, **217**, 295.
17 Z. Chen, S. Jiang, G. Kang, D. Nguyen, G. C. Schat and R. P. Van Duyne, *J. Am. Chem. Soc.*, 2019, **141**(39), 15684.
18 L. Acuña-Saavedra, A. M. Méndez-Torres, G. Cárdenas-Jirón, R. Oñate, B. Sánchez-Allende, R. Venegas, R. Bernal, F. Melo, E. Imbarack, J. H. Zagal and I. Ponce, *ACS Catal.*, 2025, **15**(2), 719.
19 F. Demir, H. Y. Yenilmez, A. Koca and Z. A. Bayır, *J. Solid State Electrochem.*, 2022, **26**, 761.
20 B. B. Carbas, S. Özbakır and Y. Kaya, *Synth. Met.*, 2023, **293**, 117298.
21 N. Blouin, A. Michaud and M. Leclerc, *Adv. Mater.*, 2007, **19**, 2295.
22 F. B. Koyuncu, E. Sefer, S. Koyuncu and E. Ozdemir, *Macromolecules*, 2011, **44**, 8407.
23 J. F. Ambrose and R. F. Nelson, *J. Electrochem. Soc.*, 1968, **115**, 1159.
24 A. Ghosh, E. J. Ra, M. Jin, H.-K. Jeong, T. H. Kim, C. Biswas and Y. H. Lee, *Adv. Funct. Mater.*, 2011, **21**, 2541.
25 (*a*) P. Khoza, E. Antunes and T. Nyokong, *Polyhedron*, 2013, **61**, 119; (*b*) P. Khoza, E. Antunes and T. Nyokong, *Dyes Pigm.*, 2014, **104**, 57; (*c*) N. Farajzadeh, H. Y. Yenilmez, D. Bahar, N. G. Kuşçulu, E. K. Selvi and Z. A. Bayır, *Dalton Trans.*, 2023, **5**, 94144.
26 S. Banerjee, B. Mordina, P. Sinha and K. K. Kar, *J. Energy Storage*, 2025, **108**, 115075.
27 B. Yıldız, E. Ahmetali, Ö. Budak, A. Koca and M. K. Şener, *New J. Chem.*, 2022, **46**, 7410.
28 D. AlMarzouq, S. A. Majeed, Ö. Budak and A. Koca, *Inorg. Chim. Acta*, 2021, **527**, 120558.
29 I. Gusev, M. Ferreira, D.-L. Versace, S. Abbad-Andaloussi, S. Pluczyk-Małek, K. Erfurt, A. Duda, P. Data and A. Blacha-Grzechnik, *Materials*, 2022, **15**, 975.

30 L. Dong, W. Zhao, T. Liu, L. Sun and X. Li, *J. Electroanal. Chem.*, 2022, **921**, 116658.
31 Yu J. Yang, M. Liu, C. Jiang, P. Yang, N. Wang, S. Chen and Y. Cheng, *J. Energy Storage*, 2021, **44**, 103462.
32 A. Ali, I. Hameed, I. Hussain, R. Mujahid, R. T. M. Ahmad, Z. Yahya, M. Waqas and M. Ammar, *J. Mater. Sci.: Mater. Electron.*, 2023, **34**, 744.
33 C. Zhou, Q. Wang, X. Yan, J. Wang, D. Wang, X. Yuan, H. Jiang, Y. Zhu and X. Cheng, *Ceram. Int.*, 2020, **46**, 15385.
34 H. Y. Yenilmez, N. F. Öztürk, Ö. Budak, Ö. İ. Öney, A. Koca and Z. A. Bayır, *Chem. – Asian J.*, 2024, **19**, e202400938.
35 N. P. Kumar, T. Sharanakumar and K. V. Reddy, *Chem. Pap.*, 2021, **75**, 2683.
36 Y. Wang, M. Li, R. Ramachandran, H. Shan, Q. Chen, A. Luo, F. Wang and Z.-X. Xu, *J. Energy Chem.*, 2023, **76**, 214.
37 Y. Chen, L. Tong, G. Lin and X. Liu, *Mater. Chem. Phys.*, 2022, **277**, 125433.